SCIENTIFIC REPORTS

OPEN

SUBJECT AREAS:
INORGANIC LEDS
OPTICS AND PHOTONICS

Received
7 May 2014

Accepted
3 July 2014

Published
25 July 2014

Correspondence and requests for materials should be addressed to T.G.K. (tgkim1@korea.ac.kr)

Fabrication of wide-bandgap transparent electrodes by using conductive filaments: Performance breakthrough in vertical-type GaN LED

Su Jin Kim[1], Hee-Dong Kim[1], Kyeong Heon Kim[1], Hee Woong Shin[1], Il Ki Han[2] & Tae Geun Kim[1]

[1]School of Electrical Engineering, Korea University, Anam-dong 5-ga, Sungbuk-gu, Seoul 136-701, Republic of Korea, [2]Nano Device Research Center, Korea Institute of Science and Technology, Seoul, 136-791, Republic of Korea.

For realizing next-generation solid-state lighting devices, performance breakthroughs must be accomplished for nitride-based light-emitting diodes (LEDs). Highly transparent conductive electrodes (TCEs) may be key to achieving this goal, as they provide uniform current injection and distribution across a large device area, eventually increasing the light output power. However, the trade-off between electrical conductivity and optical transmittance of LEDs must be addressed. Herein, we introduce a novel strategy based on TCEs fabricated using wide-bandgap (WB) materials such as SiN_x, incorporated beneath the n-type electrode of vertical-type LEDs, and show the feasibility of this strategy. We employ a novel electrical breakdown (EBD) technique to form conductive filaments (or current paths) between a TCE and *n*-GaN (GaN: gallium nitride). By employing the EBD process, we obtain both ohmic behavior for SiN_x TCE/*n*-GaN and a current spreading effect across *n*-GaN. These results demonstrate the tremendous potential of WB-TCEs for use in high-performance optoelectronic devices.

Gallium nitride (GaN)-based light-emitting diodes (LEDs) have been extensively researched as optoelectronic devices for illumination in applications such as automotive headlights, full-color displays, and interior/exterior lighting[1–8]. Nevertheless, traditional incandescent and fluorescent lamps have relatively low optical output power, and replacing them remains a challenge[9]. To realize high-power and high-efficiency LEDs, uniformly distributed current injection and a large chip size are important technological requirements[1,10]. Tremendous efforts on improving current injection and distribution have led to the introduction of transparent conducting electrodes (TCEs) such as indium tin oxide (ITO)[11,12], Ga-doped zinc oxide[13], and graphene films[14,15]. Moreover, vertical-type light-emitting diodes (VLEDs) have been widely used because of their advantages, including larger emitting areas and better current spreading than traditional lateral-type LEDs[16,17]. However, under high current operations, the current injected into a *n*-GaN layer does not sufficiently spread over the entire surface, thereby leading to non-uniform light emission and reduced luminous efficiency[3,15,18]. To overcome this drawback, several approaches including the use of uniformly designed *n*-type electrode patterns[19], insulating current blocking layers in *p*-GaN[20], and *n*-type TCEs such as ITO[21] and indium zinc oxide (IZO)[22] have been proposed for effective current spreading. However, the increase in light absorption due to the relatively narrower bandgap of ITO- and IZO-based TCEs limits light extraction from the chip surface. The use of graphene films as TCEs in LEDs has been reported, but these LEDs show deteriorated electrical properties owing to a high contact barrier and high resistance[14,23]. Therefore, a novel TCE with high transmittance and low contact resistance must be developed to realize performance improvements for high-power LEDs.

Recently, we demonstrated a novel method[24] for achieving both high electrical conductivity and high optical transmittance by applying the electrical breakdown (EBD) process on wide-bandgap (WB) materials such as SiN_x. In this study, we successfully applied this method to the N-face *n*-GaN (denoted hereafter as *n*-GaN) layer of a GaN-based VLED.

Results

Fig. 1a presents a schematic view of a VLED with WB-TCEs under EBD; the magnified figure shows that conducting filaments (CFs) can be formed via nitrogen vacancies in the WB-TCEs to provide a current path

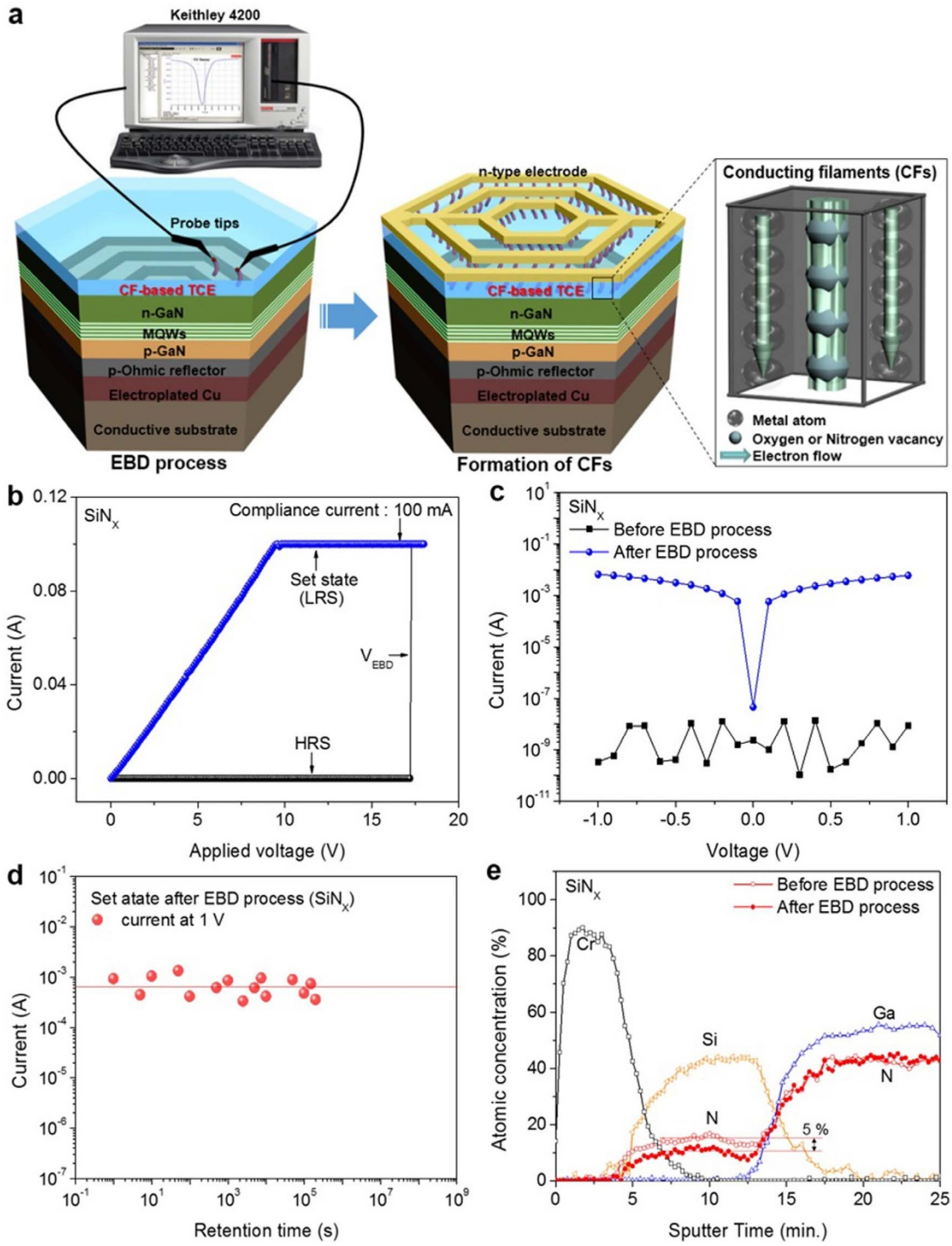

Figure 1 | **Schematic illustrations of GaN-based VLED with CF-based TCEs and their electrical conduction mechanism.** (a), Schematic view of GaN-based VLED with CF-based TCEs after EBD; the zoom-in figure shows that CFs can be formed within TCEs. (b,c), Current–voltage characteristic curves measured for a 20-nm-thick SiN_x TCE before and after EBD. (d), Long-term stability of LRS at 1 V as a function of retention time. (e), Nitrogen concentration of SiN_x films and at the interface between the SiN_x TCE and *n*-GaN layer before and after EBD, as determined by Auger electron spectroscopy.

between the TCEs and *n*-GaN. The details of VLED fabrication steps are illustrated in Fig. S1 of Supplementary Information. To obtain conductivity through the formation of CFs in the SiN_x TCEs, we performed a DC voltage sweep from 0 to 18 V between two-point probe contacts on SiN_x/*n*-GaN along the current-blocking patterns of the *p*-GaN side using a Keithley 4200 parameter analyzer (Fig. 1b). During voltage application, the current remained in the high-resistance state (HRS), which was maintained up to 17.4 V. However, a sharp rise in the current occurred at 17.4 V (V_{EBD}). A current compliance of 100 mA (blue line) was imposed during the EBD process to prevent severe damage. We then confirmed that the current increased linearly with increasing bias and reached a maximum compliance value of 100 mA at a bias of >9.6 V. This sudden transition from HRS to the low-resistance state (LRS) indicates

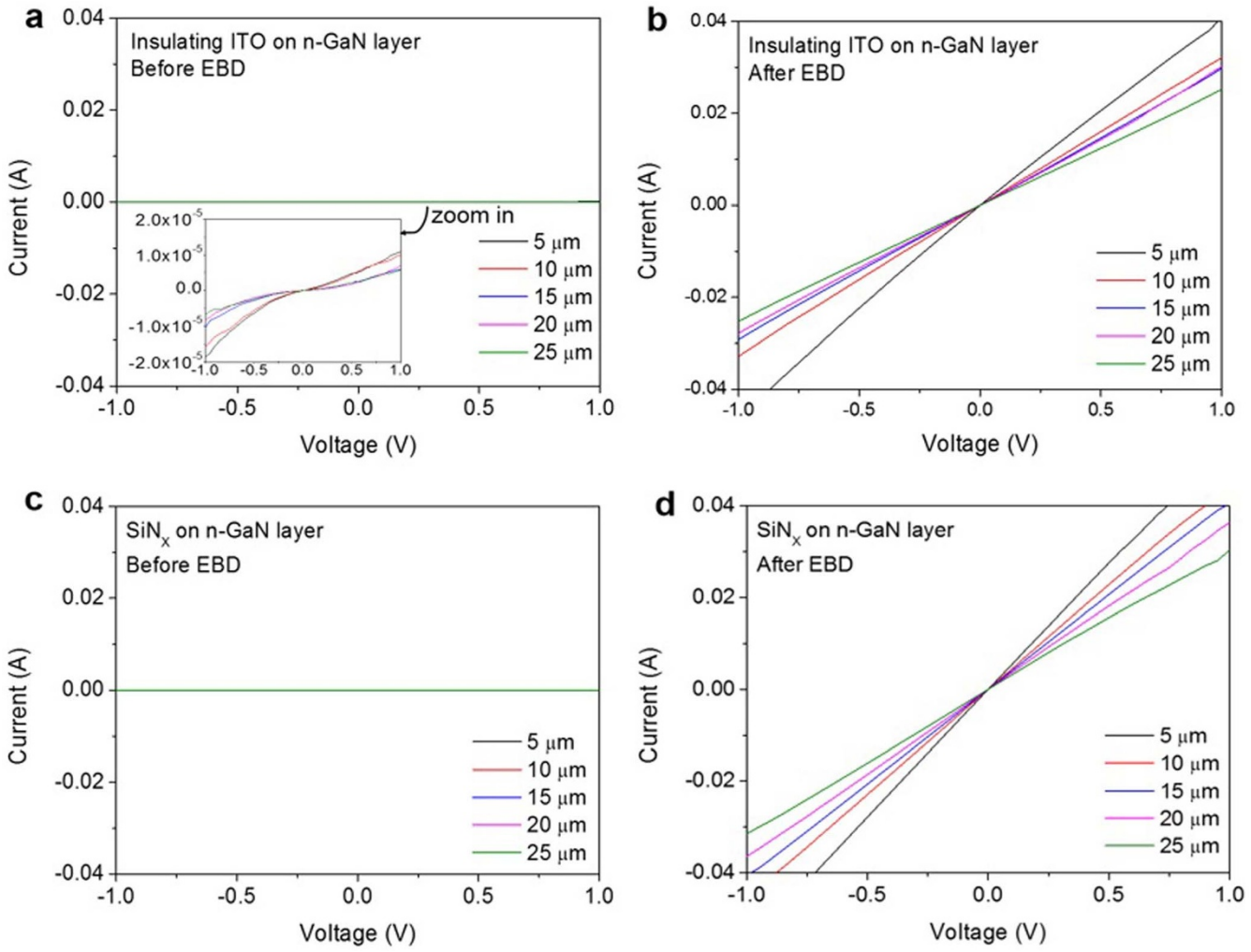

Figure 2 | Comparison of electrical characteristics of proposed CF-based TCEs on *n*-GaN layers before and after EBD. (a,b), *I–V* characteristic curves measured for different pad spacings of insulating ITO deposited on *n*-GaN layers (a) before and (b) after EBD. (c,d), *I–V* characteristic curves measured for different pad spacings of insulating ITO deposited on *n*-GaN layers (c) before and (d) after EBD.

that CFs, often observed in resistance-change memory materials, were formed in SiN_x TCEs after EBD. Further, it was found that the current level at 1 V increased from a few nanoamperes to ~5.9 mA after EBD (Fig. 1c). The EBD process for metallic and insulating ITO is shown in Figs. S2 and S3 of Supplementary Information. To investigate the long-term stability of electrical conductivity, retention at 1 V was measured (Fig. 1d). The extrapolated result against the delay time indicated that LRS could be maintained for $>10^6$ s and that the aging behavior of conductivity would be stable, which indicates that the CFs generated by EBD are sufficiently reliable for device applications as TCEs. To ascertain CF formation as an electrical path, the change in the N atomic concentration in SiN_x films was investigated by Auger electron spectroscopy before and after EBD (Fig. 1e). After EBD, the N concentration in the SiN_x TCE decreased by ~5%, indicating that the EBD process can facilitate the formation of active N-deficient regions (origin of CFs) in the SiN_x TCE, which is responsible for significant increase in conductivity. This result is quite similar to the presence of N (or O) vacancies acting as conducting paths within films of resistive-switching memory devices[25–27]. Our group has observed the formation of CFs after EBD using a conductive atomic force microscopy (C-AFM) analysis[27–29], which was consistent with previously reported data measured from transmission electron microscopy (TEM)[26,30–32] and C-AFM[25,33–35] approaches.

Discussion

Contact resistance and optical transmittance are crucial factors for realizing efficient current injection and light extraction, considering device performance. Hence, the specific contact resistances (ρ_c) of CF-based TCEs/*n*-GaN were first investigated using a transmission line model (TLM) measurement (Figs. 2a–2d). Before EBD, the current–voltage (*I–V*) characteristics of both insulating ITO and SiN_x TCE contacts on *n*-GaN were non-linear (Figs. 2a and 2c). This is attributed to the large Schottky barrier height (SBH) between the TCE and *n*-GaN, as well as the low intrinsic conductivity of the TCEs. However, after EBD, we achieved linear ohmic characteristics with a low ρ_c of $1.15 \times 10^{-4}\ \Omega\cdot cm^2$ and $8.23 \times 10^{-5}\ \Omega\cdot cm^2$ for the insulating ITO and SiN_x, respectively (Figs. 2b and 2d). The ρ_c calculation was deduced from the intercept of the plot for total resistance versus pad spacing (Figs. S4a and S4b of Supplementary Information). These values are comparable to the ρ_c of metals on *n*-GaN (Figs. S4c and S4d of Supplementary Information). These improved ohmic behaviors could be explained by the reduced SBH between the TCE and *n*-GaN due to the locally generated energy levels in the SiN_x (or ITO) TCE in relation to CFs, which allows effective carrier injection from the metal to *n*-GaN via CFs (Fig. S5 of Supplementary Information).

Next, the optical transmittances of the metallic ITO, insulating ITO, and SiN_x TCEs on quartz substrates were measured to be 86.9, 93.2, and 97.7% at 460 nm, respectively (Figs. 3a and 3b).

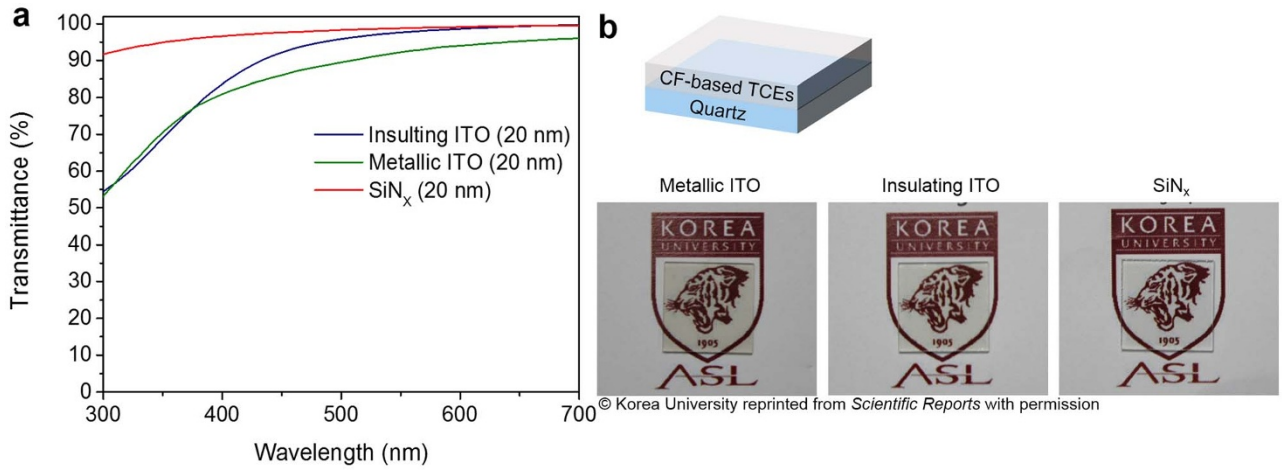

Figure 3 | Optical transmittance of proposed TCEs after EBD. (a), Optical transmission spectra of proposed TCE layers on quartz substrates in the wavelength range of 300–700 nm. (b), Photograph of each sample placed on a background logo. The upper figure shows the structure of the samples in the photographs.

These results indicate that the CF-based SiN_x TCE is suitable for use as transparent ohmic contacts to *n*-GaN.

Finally, we fabricated VLEDs to demonstrate the validity of the proposed concept on the basis of device performance, and compared the *I–V*, reverse leakage current, and light output power characteristics of a conventional VLED and those of VLEDs with metallic ITO, insulating ITO, and SiN_x TCEs after EBD (Figs. 4a and 4b). Interestingly, the lowest forward voltage and series resistance were observed for VLED with SiN_x, and VLED with insulating ITO also showed lower values than the conventional VLED, which directly show the effectiveness of our CF-based ohmic method. The forward voltages measured for the above four samples were 3.93, 4.55, 3.76, and 3.43 V at 350 mA in order, while the series resistances calculated from the slope of the *I–V* curves were 1.88, 2.84, 2.07, and 1.58 Ω, respectively (Fig. 4a). Herein, the forward voltage was measured for a single *n*-contact before packaging; therefore, it can be further reduced for double *n*-contacts after packaging because an additional *n*-contact can mitigate current accumulation underneath the single *n*-contact pad[36]. Besides, to verify the reliable operation of VLEDs with CF-based TCEs, we measured reverse leakage currents during a voltage sweep from 0 to −10 V, as shown in the inset of Fig. 4a. It is found that the leakage currents at a reverse voltage of 10 V are approximately 5.2, 4.26, 5.3, 3.91 μA for conventional VLEDs and VLEDs with metallic ITO, insulating ITO, and SiNx TCEs after EBD, respectively. These leakage values ranging from 3.91 to 5.3 μA are sufficiently low for reliable operation of VLEDs. The sample-to-sample variations in leakage currents were negligible for all VLEDs. This result indicats that the EBD process used for CF generation in WB-TCEs does not cause any severe damages in device performance. We also observed the highest light output power for VLEDs with SiN_x, and its value measured at 1 A was higher by 9.0, 21.7, and 10.2% than that of the conventional VLED and VLEDs with metallic ITO and insulating ITO, respectively (Fig. 4b). The output powers of VLEDs with metallic- and insulating-ITO were lower than that of the conventional VLED due to the light absorption via ITO. In particular, the VLED with SiN_x exhibited little degradation in the light output power even at 1 A, thereby suggesting the possibility of its application to high-power LEDs (>1 W). These improvements can be attributed to the introduction of the CF-based SiN_x TCE that led to (i) high transmittance (Fig. 3a); (ii) better current injection/distribution over the entire *n*-GaN surface; (iii) graded index effects between *n*-GaN and air. To verify these assumptions, we measured the light emission images of the four samples, as shown in Fig. 4c; the VLED with the SiN_x TCE showed the brightest and most uniform light emission at 50 and 150 mA. This result might be due to effective current injection and spreading from the metal to *n*-GaN via CFs formed in pyramid (or branchlike) shape[32,37] across the SiN_x TCE. We also performed a three-dimensional finite-difference time-domain simulation to verify the graded index effect of the light output power in VLEDs (Fig. S6 of Supplementary Information). The VLED with the SiN_x TCE showed the strongest light extraction; this result can be attributed to the reduced total internal reflection at the GaN/air interface and slightly broad light emitting patterns from GaN to air.

In summary, we have successfully demonstrated that our newly developed CF-based WB-TCEs are practically effective for forming direct ohmic contacts to *n*-GaN, and that their use would result in performance breakthroughs for GaN-based VLEDs. We employed CF-based SiN_x TCEs as *n*-type transparent conductive layers and compared the performance of a conventional VLED with those of VLEDs containing metallic and insulating ITO; the results showed that forward voltages substantially decreased from 3.93 to 3.43 V at 350 mA (for a single n-contact) while the output power increased from 19.98 to 21.77 mW at 1 A. These results not only show the feasibility of using our CF-based WB TCE as a replacement for conventional ITO in the visible regime but also significant progress is expected for ultraviolet (UV) LEDs because of its higher transmittance in the UV regime.

Methods

Fabrication of GaN-based VLEDs with WB-TCEs. Hexagonally shaped blue VLEDs emitting at ~460 nm (dimensions: ~1 mm × 1 mm) were fabricated on LED templates. A GaN-based LED structure was grown by metal-organic chemical vapor deposition on (0001)-oriented sapphire substrates. As shown in Fig. S1 of Supplementary Information, the LED templates (epistructures) consisted of a 2-μm-thick undoped GaN buffer layer, a 3.5-μm-thick Si-doped *n*-type GaN layer, five pairs of InGaN/GaN multiquantum wells (MQWs), a 20-nm-thick *p*-type AlGaN electron-blocking layer, and a 150-nm-thick Mg-doped *p*-type GaN layer. The VLED samples were treated with a piranha solution (H_2SO_4/H_2O_2 = 1 : 1) for 5 min to remove surface oxides and organic residues. For the deposition of a SiO_2 current-blocking layer (CBL), CBL structures with geometry similar to that of the *n*-electrode were patterned on the epiwafer by using a conventional photolithography technique. After HCl treatment, SiO_2 (1400 Å) was deposited by radio-frequency (RF) magnetron sputtering under a base pressure of ~2×10^{-7} Torr and a working pressure of ~3×10^{-3} Torr. A Ag-based reflective *p*-type ohmic contact was then deposited on *p*-type GaN, followed by annealing at 500°C for 1 min in ambient nitrogen. A Ni/Au seed layer was deposited, and the 100-mm-thick copper layer was then electroplated. Afterward, the whole wafer (LED epistructures) was bonded to a support substrate (receptor) by using an ethyl cyanoacrylate ($C_6H_7NO_2$)-based adhesive. Subsequently, sapphire was separated from the LED structure by using a laser lift-off (LLO) system with KrF pulsed excimer laser (ELMS 1000, QMC Inc.). After the LLO process, the samples were treated with a HCl solution (HCl/DI = 1 : 1) for 3 min to remove residual Ga droplets on the exposed undoped GaN surface. Undoped GaN was then

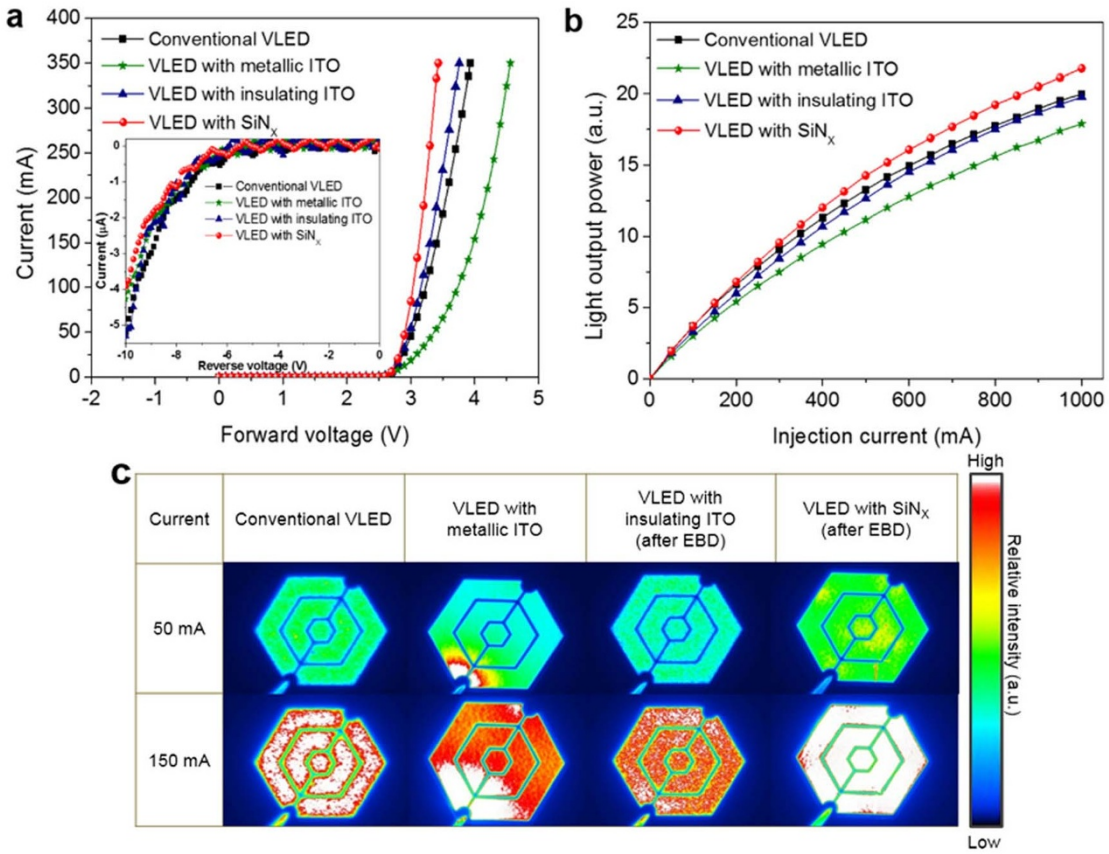

Figure 4 | Performance and light emission images of VELDs with conventional metal electrode and with CF-based TCEs before and after EBD. (a), Current–voltage characteristics of conventional VLEDs and VLEDs with different TCEs. Inset shows reverse leakage current characteristics of conventional VLEDs and VLEDs with different TCEs. (b), Light output power versus injection current characteristics for conventional VLEDs and VLEDs with different TCEs. (c), Microscopic light emission photographs of different VLED chip surfaces. The light emission images were obtained at injection currents of 50 and 150 mA for clear comparison. Relative light emission intensities are indicated by the color bar located in the right-hand side of the light emission images.

removed using inductively coupled plasma (ICP) etching. Standard photolithography and ICP-RIE processes employed thereafter defined isolated hexagonally shaped mesa structures. Subsequently, 20-nm-thick TCE films such as those of metallic ITO, insulating ITO, and SiN_x with isolated mesa structures were deposited on the *n*-GaN layers by using the RF magnetron sputtering system in ambient $Ar–O_2$ (or $Ar–N_2$) gas at a base pressure of $\sim 2 \times 10^{-7}$ Torr and a working pressure of $\sim 3 \times 10^{-3}$ Torr. Subsequently, the EBD process involving the application of electrical voltages was conducted along the current-blocking patterns of the *p*-GaN side in VLEDs to form conducting filaments (CFs), providing a current path between WB-TCEs and *n*-GaN (more details for the EBD processes are given in Fig. 2). Finally, Cr/Ni/Au was deposited on the *n*-GaN surface as an *n*-type electrode by electron-beam evaporation. For comparison, VLEDs without WB-TCEs (denoted as conventional VLEDs) were also prepared using the same LED epitaxial wafer under the same fabrication conditions.

Electrical and optical measurements. First, a transmission line model (TLM) measurement was used to evaluate the ohmic contact capability of the proposed CF-based TCEs deposited on both *n*-GaN layers. The electron concentration of the *n*-GaN sample was 1×10^{19} cm^{-3}. To fabricate TLM patterns, mesa isolation was first performed using an inductively coupled plasma etcher. Then, the TLM patterns of the contact pad (100 × 100 μm) with varied spacing from 5 to 25 μm were defined by photolithography and an additional development process. Next, 20-nm-thick TCE films such as those of insulating ITO and SiN_x with isolated mesa structures were deposited on the *n*-GaN layers using the RF magnetron sputtering system in ambient $Ar–O_2$ (or $Ar–N_2$) gas at a base pressure of $\sim 2 \times 10^{-7}$ Torr and a working pressure of $\sim 3 \times 10^{-3}$ Torr. Afterward, a lift-off process was performed using acetone. The current–voltage characteristics of the contacts were measured using a Keithley 4200 semiconductor parameter analyzer.

Next, to quantitatively evaluate the transmittance of the proposed CF-based TCEs, 20-nm-thick TCE films such as those of metallic ITO, insulating ITO, and SiN_x were deposited on quartz substrates using the RF sputtering system. The film deposition was performed for each TCE target in ambient $Ar–O_2$ (or $Ar–N_2$) gas at a base pressure of $\sim 2 \times 10^{-7}$ Torr and a working pressure of $\sim 3 \times 10^{-3}$ Torr. The transmittance of the TCE films on quartz substrates was then measured as a function of wavelength by using a Lambda 35 UV/VIS spectrometer with an operating wavelength range from 190 to 1100 nm.

Finally, the light output power and forward voltage were measured for full-structure LED chips by using a wafer-level LED measurement system (OPI-150, WithLight Co., Ltd.). More specifically, the light output power of each LED was measured from the top side of the LEDs by using a Si photodiode connected to an optical power meter. Light-emission images of the VLED chip surface were acquired using a photoemission microscope.

1. Chu, C.-F. *et al.* High Brightness GaN Vertical Light-Emitting Diodes on Metal Alloy for General Lighting Application. *Proc. IEEE* **98**, 1197–1207 (2010).
2. Wierer, J. J., David, A. & Megens, M. M. III-nitride photonic-crystal light-emitting diodes with high extraction efficiency. *Nature Photon.* **3**, 163–169 (2009).
3. Malyutenko, V. K., Bolgov, S. S. & Tykhonov, A. N. Research on Electrical Efficiency Degradation Influenced by Current Crowding in Vertical Blue InGaN-on-SiC Light-Emitting Diodes. *IEEE Photon. Technol. Lett* **24**, 1124–1126 (2012).
4. Kuang, P. *et al.* Constant, K. A New Architecture for Transparent Electrodes: Relieving the Trade-Off Between Electrical Conductivity and Optical Transmittance. *Adv. Mater.* **23**, 2469–2473 (2011).
5. O'Dwyer, C. *et al.* Bottom-up growth of fully transparent contact layers of indium tin oxide nanowires for light-emitting devices. *Nature Nanotechnol.* **4**, 239–244 (2009).
6. Pimputkar, S., Speck, J. S., DenBaars, S. P. & Nakamura, S. Prospects for LED lighting. *Nature Photon.* **3**, 180–182 (2009).
7. DenBaars, S. P. *et al.* Development of gallium-nitride-based light-emitting diodes (LEDs) and laser diodes for energy-efficient lighting and displays. *Acta Materialia* **61**, 945–951 (2013).
8. Tan, S. T., Sun, X. W., Demir, H. V. & DenBaars, S. P. Advances in the LED Materials and Architectures for Energy-Saving Solid-State Lighting Toward "Lighting Revolution". *IEEE Photonics Journal* **4**, 613–619 (2012).
9. Crawford, M. H. LEDs for Solid-State Lighting: Performance Challenges and Recent Advances. *IEEE J. Sel. Top. Quantum Electron.* **15**, 1028–1040 (2009).

10. Huang, S. *et al.* Lateral Current Spreading Effect on the Efficiency Droop in GaN Based Light-Emitting Diodes. *J. Disp. Technol.* **9**, 266–271 (2013).
11. Chae, D. J. *et al.* AlGaN-based ultraviolet light-emitting diodes using fluorine-doped indium tin oxide electrodes. *Appl. Phys. Lett* **100**, 081110 (2012).
12. Helander, M. G. *et al.* Chlorinated indium tin oxide electrodes with high work function for organic device compatibility. *Science* **332**, 944–947 (2011).
13. Park, T.-Y. *et al.* Enhanced optical power and low forward voltage of GaN-based light-emitting diodes with Ga-doped ZnO transparent conducting layer. *Appl. Phys. Lett* **96**, 051124 (2010).
14. Kim, B.-J. *et al.* Large-area transparent conductive few-layer graphene electrode in GaN-based ultra-violet light-emitting diodes. *Appl. Phys. Lett* **99**, 143101 (2011).
15. Wang, L. *et al.* Partially sandwiched graphene as transparent conductive layer for InGaN-based vertical light emitting diodes. *Appl. Phys. Lett* **101**, 061102 (2012).
16. Shchekin, O. B. *et al.* High performance thin-film-flip-chip-InGaN-GaN light-emitting diodes. *Appl. Phys. Lett* **89**, 071109 (2006).
17. Liu, W.-J. *et al.* Low-temperature bonding technique for fabrication of high-power GaN-based blue vertical light-emitting diodes. *Opt. Mater.* **34**, 1327–1329 (2012).
18. Chen, T.-M. *et al.* Use of anisotropic laser etching to the top n-GaN layer to alleviate current-crowding effect in vertical-structured GaN-based light-emitting diodes. *Appl. Phys. Lett* **90**, 041115 (2007).
19. Kim, H. *et al.* Design of high-efficiency GaN-based light emitting diodes with vertical injection geometry. *Appl. Phys. Lett* **91**, 023510 (2007).
20. Son, J. H. *et al.* Enhancement of wall-plug efficiency in vertical InGaN/GaN LEDs by improved current spreading. *Opt. Express* **20**, A287–A292 (2012).
21. Kim, D. W., Lee, H. Y., Yoo, M. C. & Yeom, G. Y. Highly efficient vertical laser-liftoff GaN-based light-emitting diodes formed by optimization of the cathode structure. *Appl. Phys. Lett* **86**, 052108 (2005).
22. Wang, S.-J. *et al.* The use of transparent conducting indium-zinc oxide film as a current spreading layer for vertical-structured high-power GaN-based light-emitting diodes. *IEEE Photon. Technol. Lett* **18**, 1146–1148 (2006).
23. Jo, G. *et al.* Large-scale patterned multi-layer graphene films as transparent conducting electrodes for GaN light-emitting diodes. *Nanotechnol.* **21**, 175201 (2010).
24. Kim, H.-D. *et al.* A Universal Method of Producing Transparent Electrodes Using Wide-Bandgap Materials. *Adv. Funct. Mater.* **24**, 1575–1581 (2014).
25. Mehonic, A. *et al.* Electrically tailored resistance switching in silicon oxide. *Nanotechnol.* **23**, 455201 (2012).
26. Yang, Y. *et al.* Observation of conducting filament growth in nanoscale resistive memories. *Nat. Commun.* **3**, 732 (2012).
27. Kim, H.-D., An, H.-M., Kim, E. B. & Kim, T. G. Stable Bipolar Resistive Switching Characteristics and Resistive Switching Mechanisms Observed in Aluminum Nitride-based ReRAM Devices. *IEEE Trans. Electron Devices* **58**, 3566–3573 (2011).
28. Kim, H.-D. *et al.* Large resistive-switching phenomena observed in Ag/Si3N4/Al memory cells. *Semicond. Sci. Technol.* **25**, 065002 (2010).
29. Kim, H.-D., An, H.-M., Hong, S. M. & Kim, T. G. Unipolar resistive switching phenomena in fully transparent SiN-based memory cells. *Semicond. Sci. Technol.* **27**, 125020 (2012).
30. Park, G.-S. *et al.* In situ observation of filamentary conducting channels in an asymmetric Ta_2O_{5-x}/TaO_{2-x} bilayer structure. *Nat. Commun.* **4**, 2382 (2013).
31. Yao, J., Zhong, L., Natelson, D. & Tour, J. M. In situ imaging of the conducting filament in a silicon oxide resistive switch. *Sci. Rep.* **2**, 242 (2012).
32. Kwon, D.-H. *et al.* Atomic structure of conducting nanofilaments in TiO_2 resistive switching memory. *Nature Nanotechnol.* **5**, 148–153 (2010).
33. Singh, B. *et al.* CAFM investigations of filamentary conduction in Cu_2O ReRAM devices fabricated using stencil lithography technique. *Nanotechnol.* **23**, 495707 (2012).
34. Yang, L. *et al.* The influence of copper top electrodes on the resistive switching effect in TiO_2 thin films studied by conductive atomic force microscopy. *Appl. Phys. Lett.* **95**, 013109 (2009).
35. Son, J. Y. & Shin, Y.-H. Direct observation of conducting filaments on resistive switching of NiO thin films. *Appl. Phys. Lett.* **92**, 222106 (2008).
36. Tu, S. H. *et al.* Characteristics of current distribution by designed electrode patterns for high power Thin GaN LED. *Solid-State Electron.* **54**, 1438–1443 (2010).
37. Ninomiya, T. *et al.* Conductive Filament Scaling of TaO_x Bipolar ReRAM for Long Retention with Low Current Operation. *Symp. VLSI Tech. Dig.* **73** (2012).

Acknowledgments

This work was supported by a National Research Foundation of Korea (NRF) grant funded by the Korean government (No. 2011-0028769). The authors thank Verticle Inc. for the supply of vertical-type GaN LEDs.

Author contributions

T.G.K. and S.J.K. conceived and designed the experiment. H.-D.K. and K.H.K. prepared the samples and S.J.K., H.-D.K., K.H.K., H.W.S. and I.K.H. conducted the experiment and simulation. T.G.K. and S.J.K. analyzed the data and wrote the manuscript. T.G.K. supervised the experiments and contributed to manuscript preparation. All authors discussed the progress of research and reviewed the manuscript.

Additional information

Supplementary information accompanies this paper at http://www.nature.com/scientificreports

Competing financial interests: The authors declare no competing financial interests.

How to cite this article: Kim, S.J. *et al.* Fabrication of wide-bandgap transparent electrodes by using conductive filaments: Performance breakthrough in vertical-type GaN LED. *Sci. Rep.* **4**, 5827; DOI:10.1038/srep05827 (2014).